Defect and Diffusion Forum Vol. 322 (2012) pp 129-150
Online available since 2012/Mar/15 at www.scientific.net
© (2012) Trans Tech Publications, Switzerland
doi:10.4028/www.scientific.net/DDF.322.129

Original Methods for Diffusion Measurements in Polycrystalline Thin Films

Alain Portavoce[1,a], Ivan Blum[1,2,b], Khalid Hoummada[2,c],
Dominique Mangelinck[1,d], Lee Chow[3,e] and Jean Bernardini[1,f]

[1]CNRS, IM2NP, Faculté des Sciences et Techniques de Saint-Jérôme, Case 142, 13397 Marseille, France

[2]Aix-Marseille Université, IM2NP, Faculté des Sciences et Techniques de Saint-Jérôme, Case 142,13397 Marseille, France

[3]Department of Physics, University of Central Florida, Orlando, Florida 32816, USA

[a]alain.portavoce@im2np.fr, [b]ivan.blum@im2np.fr, [c]khalid.hoummada@im2np.fr, [d]dominique.mangelinck@im2np.fr, [e]Lee.Chow@ucf.edu, [f]jean.bernardini@im2np.fr

Keywords: Diffusion, polycrystalline film, grain boundary, triple junction, atom probe tomography

Abstract. With the development of nanotechnologies, the number of industrial processes dealing with the production of nanostructures or nano-objects is in constant progress (microelectronics, metallurgy…). Thus, knowledge of atom mobility and the understanding of atom redistribution in nano-objects and during their fabrication have become subjects of increasing importance, since they are key parameters to control nano-fabrication. Especially, today's materials can be both composed of nano-objects as clusters or decorated defects…, and contain a large number of interfaces as in nanometer-thick film stacking and buried nano-wires or nano-islands. Atom redistribution in this type of materials is quite complex due to the combination of different effects, such as composition and stress, and is still not very well known due to experimental issues. For example, it has been shown that atomic transport in nanocrystalline layers can be several orders of magnitude faster than in microcrystalline layers, though the reason for this mobility increase is still under debate. Effective diffusion in nanocrystalline layers is expected to be highly dependent on interface and grain boundary (GB) diffusion, as well as triple junction diffusion. However, experimental measurements of diffusion coefficients in nano-grains, nano-grain boundaries, triple junctions, and interfaces, as well as investigations concerning diffusion mechanisms, and defect formation and mobility in these different diffusion paths are today still needed, in order to give a complete picture of nano-diffusion and nano-size effects upon atom transport. In this paper, we present recent studies dealing with diffusion in nano-crystalline materials using original simulations combined with usual 1D composition profile measurements, or using the particular abilities of atom probe tomography (APT) to experimentally characterize interfaces. We present techniques allowing for the simultaneous measurement of grain and GB diffusion coefficients in polycrystals, as well as the measurement of nano-grain lattice diffusion and triple junction diffusion. We also show that laser-assisted APT microscopy is the ideal tool to study interface diffusion and nano-diffusion in nanostructures, since it allows the determination of 1D, 2D and 3D atomic distributions that can be analyzed using diffusion analytical solutions or numerical simulation.

Introduction

Usually, the measurement of atom diffusion coefficients in a given matrix is performed by measuring the concentration profile of the impurity in the bulk of the matrix i) before annealing, and ii) after controlled annealing (atmosphere, time, and temperature). Then, the diffusion coefficient can be obtained by fitting the profile measured after the thermal treatment either using analytical solutions of the diffusion equation [1] or using numerical simulations [2], considering the experimental profile obtained before annealing as the initial impurity distribution. Despite that analytical solutions provide exact results over a short time scale, their use is generally limited to

All rights reserved. No part of contents of this paper may be reproduced or transmitted in any form or by any means without the written permission of TTP, www.ttp.net. (ID: 163.25.99.80-19/04/12,04:54:55)

experiments of reduced complexity (at thermodynamic equilibrium, with constant diffusion coefficients…). For example, the measurement of the diffusion coefficient of impurities in monocrystalline Si layers is often performed via numerical simulations, due to the complexity of the diffusion mechanisms (simultaneous use of interstitial and vacancy mediated mechanisms using point defects of various charge states, diffusion coefficient dependence of impurity concentration, transient diffusion out of equilibrium…) [3-5]. Furthermore, one-dimensional (1D) numerical simulations can be used to measure diffusion coefficients, and once these coefficients are known, two-dimensional (2D) simulations can be used to simulate atom diffusion in complex structures as in transistors during fabrication processes [6]. However, despite that diffusion in polycrystals is frequently simulated using finite element simulations (FES) [7-8], the measurement of diffusion coefficients in polycrystalline samples has been principally performed so far with analytical solutions of given diffusion problems [1, 9]. The model used the most is the 2D Fisher model [1] considering a diffusion source (finite or constant) on the surface of the sample that is modeled by a single grain boundary (GB) perpendicular to the surface between the two half-of-a-grain, with different constant diffusion coefficients in the GB and in the grain volume. With the solutions of this model, the GB diffusion coefficient can be measured from the 1D diffusion profiles obtained in semi-infinite samples for experiments in the Harrison's regime *B*, if the lattice diffusion coefficient (in grains) has been previously measured in the single crystal [1]. However, we show in this paper that the use of FES to measure diffusion coefficients in polycrystals can provide important benefits compared to the usual methods. For example, GB and grain diffusion coefficients can be measured simultaneously in thin films (finite thickness), without requiring the precise knowledge of the diffusion kinetic regime (*A*, *B* or *C* from Harrison), for experimental geometries of higher complexity than the Fisher model. Furthermore, FES can allow the measurement of diffusion coefficients in the bulk of nanometric grains and in triple junctions (TJ). In addition, we show that atom probe tomography (APT) microscopy combined with FES or simulations using analytical solutions can be of great use to investigate atom mobility at interfaces, GBs, and TJs.

Measurement of diffusion coefficients in polycrystalline films using FES

2D simulations: the Fisher model. In order to simulate diffusion in polycrystals taking into account the microstructure influence as grain size, GB geometry, etc. it is necessary to use a model with a 2D geometry. For example, let's consider the 2D Fisher geometry but for a film of finite size.

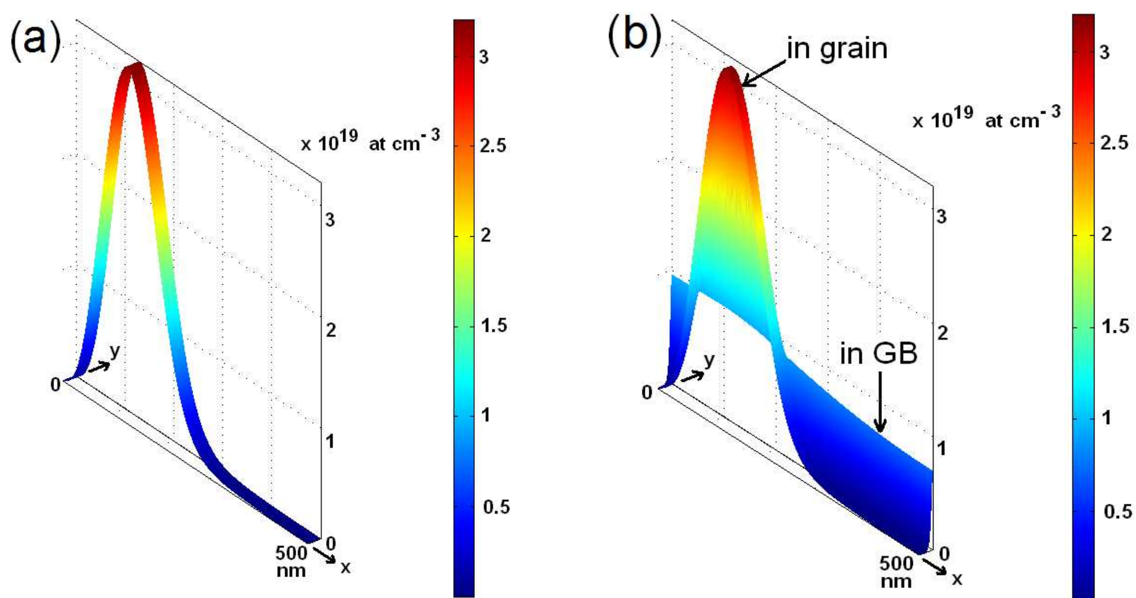

Fig. 1. Atom distribution in the 2D simulation cell: (a) initial distribution and (b) distribution after annealing simulation.

1D concentration profiles measured experimentally in a sample results from the average concentration versus depth of the two atom distributions in grains and in GBs balanced by the respective size of grains and GBs. The procedure allowing to measure the lattice and the GB diffusion coefficients in the film consists then in i) defining in the 2D model the initial distribution in grains and GBs before annealing using 1D measurements (Fig. 1a), ii) performing 2D simulations using the experimental annealing conditions as time and temperature (Fig. 1b), iii) using the 2D simulation results to define the corresponding 1D profile (Fig. 2a), iv) comparing this profile to the 1D profile measured in the sample after annealing (Fig. 2b), and v) adjusting the diffusion coefficients in the model for a new simulation in order to fit as well as possible the experimental profile with the simulated profile.

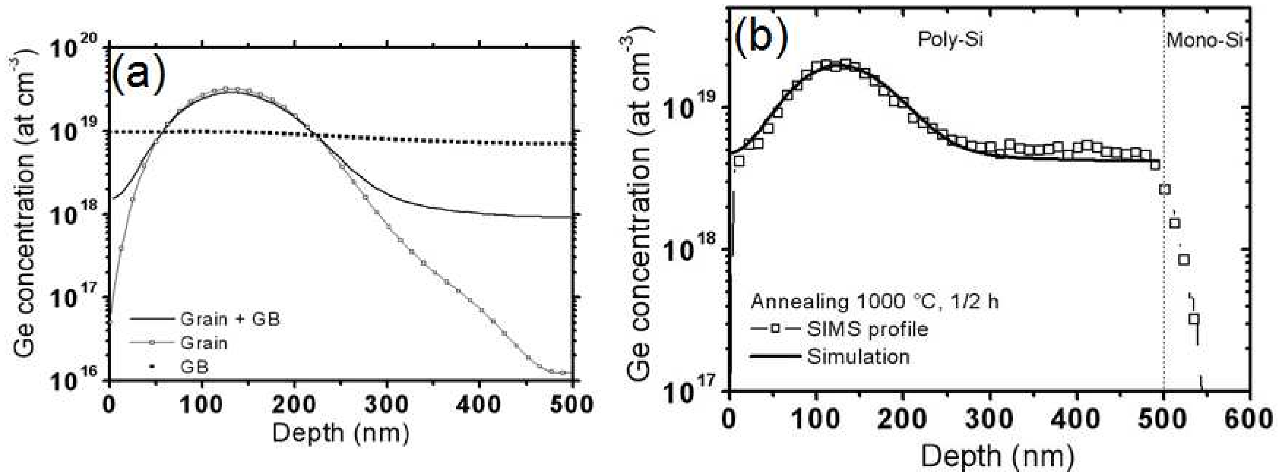

Fig. 2. 1D profiles obtained from 2D simulations: (a) diffusion profiles in the grain center (solid line and open squares) and in the GB center (solid squares) compared with the averaged profile taking into account both the grain and the GB distributions (solid line). (b) Comparison between experimental (open squares) and simulated profiles (solid line).

In the case of implanted samples, we usually consider that the distribution of implanted atoms is identical in grains and GBs. Thus, the 1D as-implanted experimental profile is entered in the 2D Fisher geometry in grains and in GBs to define the initial 2D distribution as presented in Fig. 1a. For the results presented in Figs. 1 and 2, we consider the Fisher geometry with an averaged grain width of 40 nm and a GB width of 0.5 nm on the y axis, and a layer having a thickness of 500 nm on the x axis. We found that this procedure using the 2D Fisher geometry allows to determine *simultaneously* the diffusion coefficients in grains and GBs, since these two coefficients do not affect the diffusion profile in the same way, the first part of the profile (close to the surface) being strongly dependent upon lattice diffusion, and the second part (deeper in the sample) being strongly dependent on GB diffusion [9-11]. The measurement error upon diffusion coefficients using this technique is generally comprised between 10 to 20%. This method presents several benefits: i) the GB diffusion coefficient (D_{gb}) can be measured without knowledge of the lattice diffusion coefficient (D_g), ii) it is not necessary to perform the measurements strictly in the kinetic regime B, ii) the lattice diffusion coefficient can be measured for very small diffusion lengths (few nanometers), allowing to determine the diffusion coefficient at lower temperatures than in single crystals.

2D simulations: complex geometries and complex systems. The use of FES allows to solve diffusion equations in the case of more complex problems compare to the use of diffusion equation solutions. This is especially useful for the simulations of industrial processes. For example, a first complication corresponds to the diffusion of a diluted impurity following the Fick equations of diffusion but in a sample exhibiting geometry more complex than the Fisher geometry. In this case, D_g and D_{gb} cannot always be measured simultaneously. The control of the Si dopant distribution in silicides is very important in the microelectronic fabrication processes as the electrical properties of the contact on devices can be significantly modified by dopant segregation or diffusion [12-14]. The

thickness of silicide layers is about tens of nanometers for current devices. Figure 3a presents a cross-section TEM image of a poly-Ni_2Si film encapsulated between two layers of Si oxide acting as diffusion barriers. In order to study As diffusion in this layer, As atoms have been implanted in the silicide (5×10^{15} at cm^{-2} at 120 keV). It is interesting to note that for this sample the Fisher model needed to be modified in order to take into account As diffusion at the Ni_2Si/SiO_2 interfaces (fig. 3b). Using the model presented in Fig. 3b and thanks to the procedure described earlier, we were able to measure the diffusion coefficients of As in the bulk of grains, as well as in the GBs [15-16]. Figure 4a presents the fit of experimental profiles measured by secondary ion mass spectrometry (SIMS) after annealing at 650°C for 1, 4, and 16 hours.

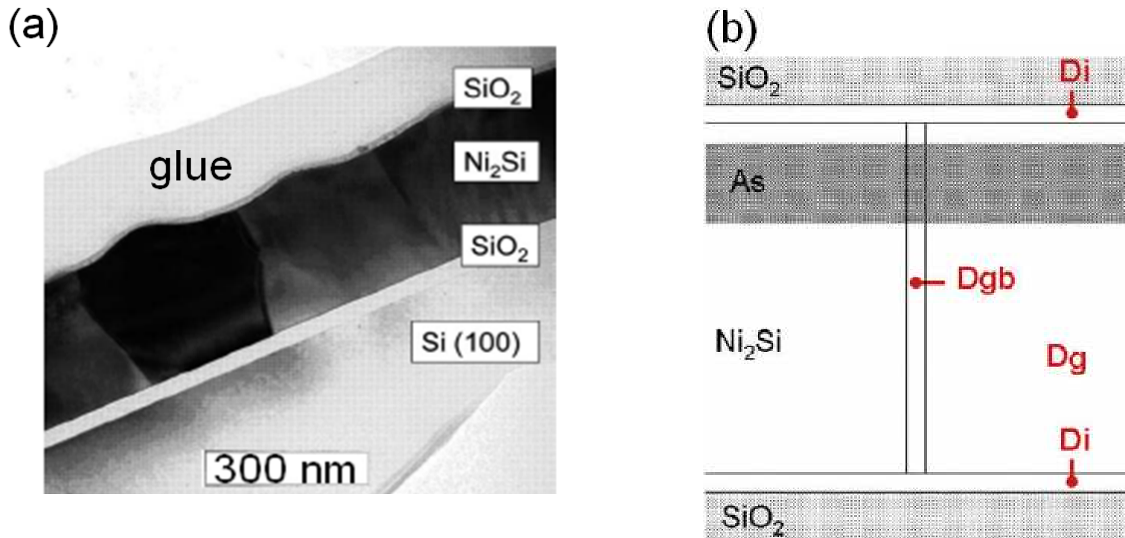

Fig. 3. TEM cross-sectional image of a Ni_2Si layer implanted with As atoms (a), and the corresponding 2D model used to measure As diffusion in this layer via 2D simulations (b).

Figure 4b presents the variation of As diffusion coefficients versus temperature both in grains and GBs in comparison with Ni self-diffusion in Ni_2Si. We found a diffusivity of 1.5×10^{-1} $\exp(-2.72\ eV/kT)$ $cm^2\ s^{-1}$ in grains and of 9.0×10^{-3} $\exp(-3.07\ eV/kT)$ $cm^3\ s^{-1}$ in GBs [15-16].

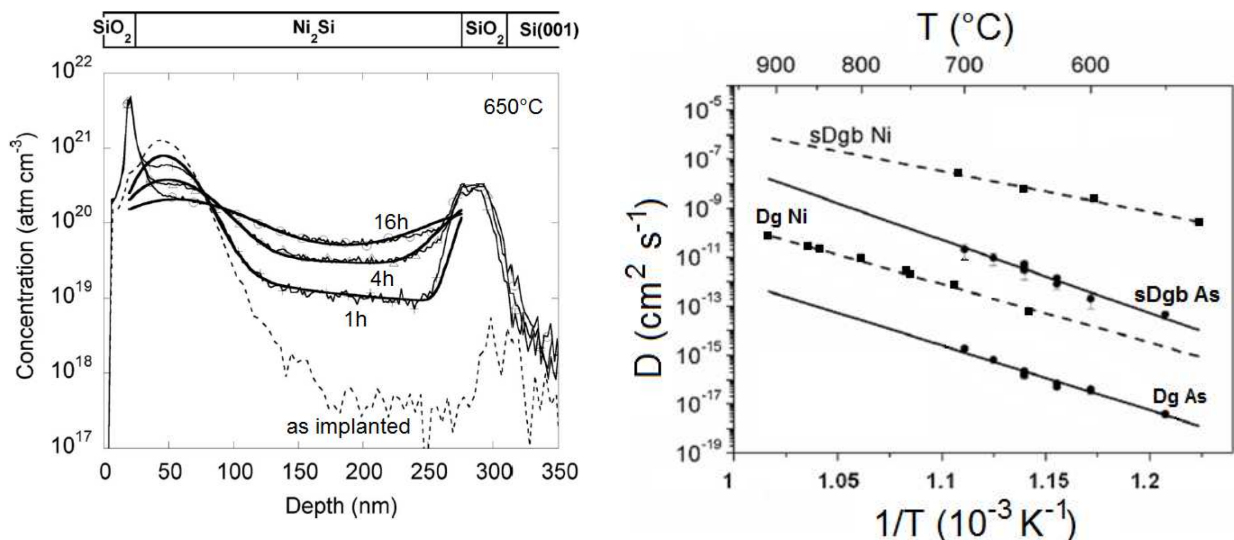

Fig. 4. Diffusion of As in a polycrystalline Ni_2Si layer located between two layers of SiO_2: (a) comparison between experimental SIMS profiles (thin lines) and simulation results (thicker lines) for annealing at 650°C, and (b) As diffusion coefficients measured in the Ni_2Si layer compared with Ni diffusion in Ni_2Si.

In this example, the lattice and GB diffusion coefficients were obtained simultaneously despite the effect of the Ni_2Si/SiO_2 interfaces. It is interesting to note that As lattice diffusion coefficients were measured over very small diffusion lengths. The fit of the three profiles presented in Fig. 4, obtained after annealing at 650°C for 1, 4 and 16 hours, gave $D_g = 1.5 \times 10^{-16}$ cm^2 s^{-1}, $D_g = 2.2 \times 10^{-16}$ cm^2 s^{-1} and $D_{gb} = 1.6 \times 10^{-16}$ cm^2 s^{-1}, respectively. These three coefficients are very close, showing that point defects in the layer were at equilibrium during annealing. Furthermore, the coefficient measured after 1h of annealing corresponds to a diffusion length in the grains of ~ 7 nm. If we had used the SIMS technique to measure As diffusion in a single crystal we could never study such a small penetration depth since it is close to the SIMS technique resolution. It is possible in our case because in regime *B* a very small diffusion depth between the grains and the GBs has a huge impact on the GBs diffusion profile. The coefficients measured after annealing for 4 and 16 hours correspond to diffusion lengths of ~ 18 and 36 nm, respectively. This confirms that the technique proposed in this paper gives relevant measurements even at low temperature for nanometer-scale diffusion lengths.

In certain cases, the microstructure of the sample can be even more complex, especially when it varies with time during thermal annealing. This is for example the case when atom redistribution takes place during GB migration. During annealing of poly-crystals, grains can grow and thus GBs can move. We usually do our best to perform diffusion experiments in conditions avoiding grain growth. However, diffusivities are often extracted from reactive diffusion experiments (oxide and silicide growth [17] for example) in order to understand phases' growth and to predict their kinetics during industrial fabrication processes (Salicide process in microelectronics for example). It is thus interesting, in some cases, to study atomic transport in GBs during grain growth, and to measure an effective diffusion coefficient. Fig. 5 presents simulation results related to the diffusion of a diluted impurity following Fick's equations in a polycrystal made of 50 nm-wide grains that are growing during thermal annealing. The simulation model uses the Fisher geometry [18] including a lateral movement of the GB, as well as an increasing grain size versus time. The model possesses three constant parameters: D_g and D_{gb}, as well as v_{gb} the GB displacement rate (or grain growth rate). If we consider that not all the grains are growing, the fraction of growing grains f_{gr} can be a fourth parameter. Of course, all these parameters cannot be measured simultaneously on a single diffusion profile.

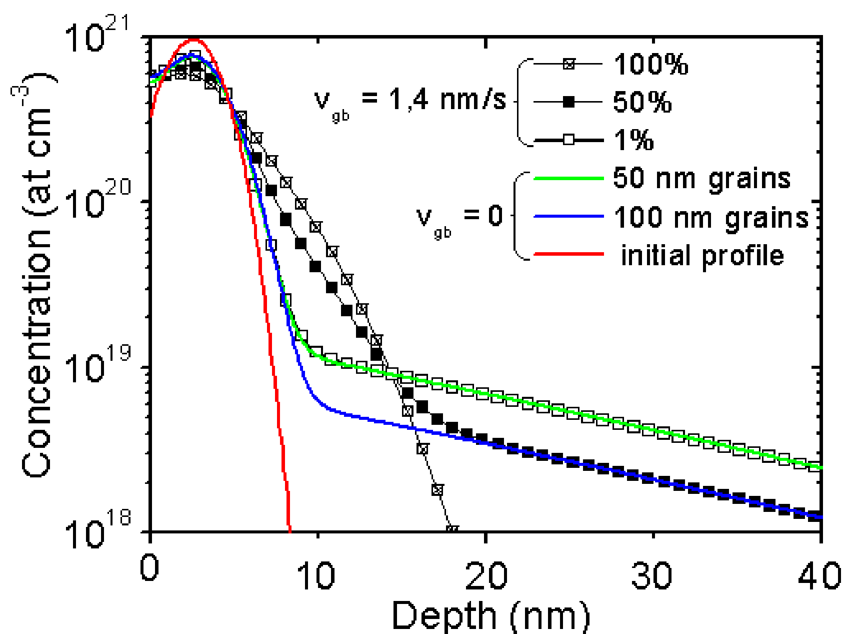

Fig. 5. 1D profiles obtained from 2D FES using the Fisher geometry with growing grains (from 50 nm to 100 nm) and moving GB, with $D_g = 2 \times 10^{-16}$, $D_{gb} = 5 \times 10^{-11}$ cm^2 s^{-1}, and $t = 3600$ s for different fraction of growing grains and v_{gb} = 0.014 nm s^{-1}.

However, v_{gb} can be measured using *in situ* X-ray diffraction for example [11], D_g can be measured individually as usual [19-20], and both introduced into the 2D model. Thus, an effective D_{gb} related to grain growth can be extracted from experiments. The results presented in Fig. 5 correspond to 1D

profiles calculated from 2D FES with $D_g = 2 \times 10^{-16}$, $D_{gb} = 5 \times 10^{-11}$ cm^2 s^{-1}, and $t = 3600$ s, in the case of 50 nm-wide grains growing up to a lateral size of 100 nm (the double of their initial size) with $v_{gb} = 0.014$ nm s^{-1}. The profiles related to diffusion in similar conditions but with grains of constant size of either 50 or 100 nm are also presented in this figure. With $v_{gb} = 0.014$ nm s^{-1}, the grains grow during the entire annealing time. If all the grains are growing (100% in Fig. 5), the diffusion profile resembles a profile corresponding to diffusion through a single phase [1], and could be misinterpreted as resulting from pure lattice diffusion, or diffusion in the kinetics regimes *A* or *C* [21]. If 1% of the grains are growing ($f_{gr} = 0.01$), the diffusion profile is superimposed on the profile corresponding to the non-growing 50 nm-wide grains. The effect of grain growth is not detectable on the diffusion profile. However, if 10% of the grains are growing ($f_{gr} = 0.1$), the grain growth effect on the profile is not negligible anymore. The modification may mislead the experimentalist that can interpret the first part of the profile, including the grain-growth related change, as resulting from lattice diffusion in grains, leading to the overestimation of D_g. One can note that in these simulations, the maximum depth of the first part of the profile is less than 20 nm, which is smaller than the critical length $5\times\sqrt{(D_g t)}$ (= 42 nm in our case) usually considered in analytical solutions as the maximum depth on experimental profiles that can reach atoms diffusing in grains. Deeper in the sample, the slopes of all the profiles are identical to the slope of the profiles of 50 and 100 nm-wide non-growing grains (except if $f_{gr} = 1$), indicating that the same diffusion coefficient can be extracted from the profile slopes using an analytical solution of the Fisher model [1]. Figure 6 presents the variations of the diffusion profile in function of the grain growth rate v_{gb}. If the grains are not growing during the entire annealing time ($v_{gb} > 0.014$ nm s^{-1}), the profile looks like to result from diffusion through a polycrystal in the kinetic regime *B*. However, it is not superimposed on either the profiles of 50 or 100 nm-wide non-growing grains. Similar to the case of growing grains during the entire annealing time, it exhibits a modified zone having a depth less than 20 nm. If v_{gb} is fast, as presented in Fig. 6 for $v_{gb} = 7$ nm s^{-1}, the grains reach a lateral size of 100 nm faster, and the deep part of the profile tends to get superimposed to the profile related to diffusion in a polycrystal of constant 100 nm-wide grains. Indeed, for fast growth rates, the grains reach a lateral size of 100 nm very rapidly, thus during the main part of the thermal treatment, the impurity diffuses in a rigid geometry with 100 nm-wide grains. Otherwise, if the grain growth rate is fast enough for the grains to reach their final size (100 nm) before the end of the thermal treatment, but slow enough for the impurity to mainly diffuse when GBs are moving, the slope of the concentration profile is different than the slope obtained in the case of immobile GBs. Thus, this slope cannot be used to extract the GB diffusion coefficient using the usual analytical solutions of diffusion [1]. In general, the slope obtained when GBs are mobile is steeper than in the case of immobile GBs.

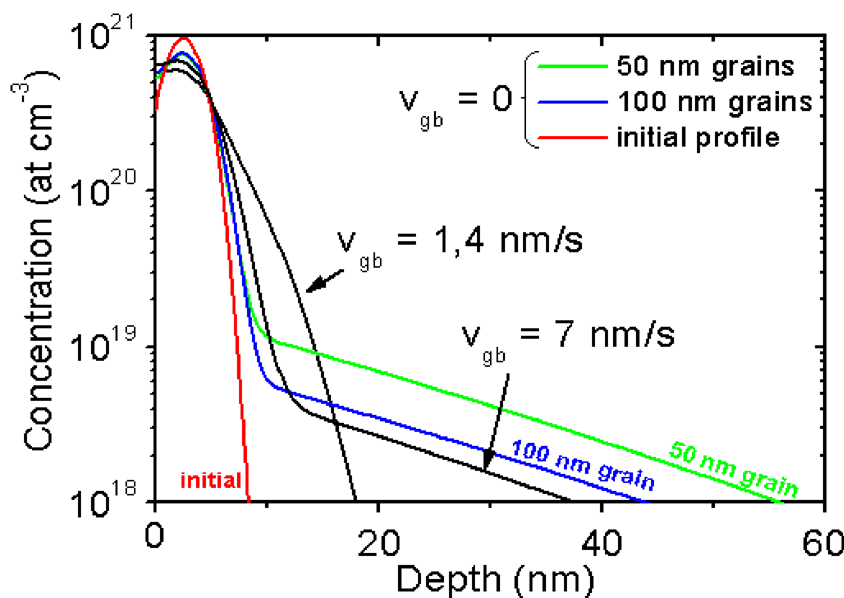

Fig. 6. 1D profiles obtained from 2D FES using the Fisher geometry with growing grain (from 50 nm to 100 nm) and moving GB, with $D_g = 2 \times 10^{-16}$, $D_{gb} = 5 \times 10^{-11}$ cm^2 s^{-1}, and $t = 3600$ s, for different grain growth rates, with all the grains growing.

In addition to geometry (or microstructure) complexity, FES can allow to extract diffusion coefficients from experimental profiles in case of impurity diffusion following more complex laws than the usual Fick's laws. For example, Fig. 7 presents simulation results concerning the diffusion of B in a 250 nm-thick Si polycrystalline film made of 50 nm-wide grains. The Si Fermi level varies with the concentration of dopant impurities as B, Ga, Al, P, As, Sb, Bi…The variation of the Fermi level generates a variation of the concentration of charged point defects. As a consequence, dopant diffusion in Si may vary with dopant concentration [22]. In addition, when dopants are activated, they are ionized and occupy substitutional sites in the Si lattice. Because the electron diffusion is faster than ion diffusion, and that electron diffusion driving forces are different from ion diffusion driving forces, the electron distribution resulting from dopant activation and the dopant distribution can create an internal electric field that can influence dopant diffusion, and varies with dopant concentration [22].

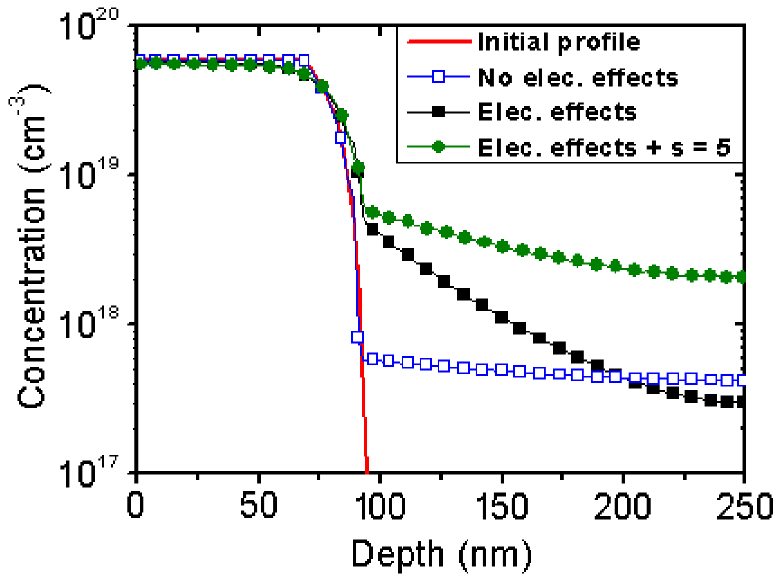

Fig. 7. Results of 2D FES concerning B diffusion in a 250 nm-thick poly-Si film using the Fisher geometry (50 nm grains) without considering the effects of charged point defects, with the charged point defect effects and considering both charged point defects as well as GB segregation with a segregation coefficient $s = 5$.

If point defect concentrations are at thermodynamically equilibrium, the dopant diffusion flux (J) in the Si grains can be written:

$$J = -hD_g \frac{dC}{dx}, \quad (1)$$

with h the factor related to the internal electric field effect, D_g the lattice diffusion coefficient, x the (1D) diffusion direction and C the dopant concentration in the grains. If all the mobile dopants are ionized:

$$h = 1 + \frac{C}{\sqrt{C^2 + 4n_i^2}}. \quad (2)$$

n_i is the electron concentration in intrinsic Si (undoped) at the considered temperature. In Si it varies with temperature as:

$$n_i = 2.16 \times 10^{16} T^{3/2} \exp\left[\frac{-0.592 + 5.12 \times 10^{-8} T^2}{kT}\right] \text{cm}^{-3}. \quad (3)$$

For p-type dopants as B, the diffusion coefficient D_g can be written as:

$$D_g = D_0 + D_{1+} \frac{p}{n_i} + D_{2+}\left(\frac{p}{n_i}\right)^2. \quad (4)$$

D_0 is the dopant diffusion coefficient related to uncharged point defects, D_{1+} is the diffusion coefficient related to point defects with a single positive charge, and D_{2+} corresponds to the diffusion coefficient related to point defects with a double positive charge. In doped Si $np = n_i^2$, and because of charge equilibrium $N_D^+ + p = N_A^- + n$, with n and p the concentrations of electrons and holes, respectively, and N_D^+ and N_A^- the concentration of activated p-type and n-type dopants, respectively. For a single p-type dopant in Si, p is related to the dopant concentration following:

$$p = \frac{C + \sqrt{C^2 + 4n_i^2}}{2}. \quad (5)$$

In GBs these electrical effects (charged point defects and internal electric field) are not considered since usually dopants in GBs do not participate in Si doping, and cannot be associated with the bulk Fermi level of Si. Furthermore, dopant diffusion in GBs has been shown to follow the usual Fick's laws [10, 19]. The simulations taking into account the electrical effects during B diffusion in poly-Si presented in Fig. 7 (solid squares) were performed using Eqs. (1) to (5) for B lattice diffusion in Si grains, and using a constant diffusion coefficient in the GBs, considering the Fisher geometry with 50 nm-wide grains and 0.5 nm-wide GBs. The B diffusion coefficients in Si and in Si GBs were taken from the literature: $D_0 = 0.123\exp(-3.37\text{ eV}/kT)$, $D_{1+} = 4.21\exp(-3.67\text{ eV}/kT)$, $D_{2+} = 39.8\exp(-4.37\text{ eV}/kT)\text{ cm}^2\text{ s}^{-1}$ [2], and $D_{gb} = 0.82\exp(-2.74\text{ eV}/kT)\text{ cm}^2\text{ s}^{-1}$ [23]. In addition, the solid circles profile in Fig. 7 corresponds to the same simulations with B segregation in GBs considering the Henry law with a segregation coefficient $s \sim 5$. These simulations correspond to annealing at 700°C for 3 hours. B atoms were allowed to diffuse only for concentrations lower than the solubility limit chosen to be 4×10^{19} at cm^{-3}. The B solubilities in grains and grain boundaries were chosen to be the same, as well as the initial profiles (solid line) in grains and grain boundaries. Without an electrical effect (open squares) we set $D_g = D_0$. The FES results are different for each case: without electrical effects, with electrical effects, and with electrical effects and GB segregation. Of course, this type of simulations is useful only if one (or few independent) model parameter(s) is (are) unknown, since all the parameters cannot be determined simultaneously. However, using the same multi-parameter model to fit profiles obtained in different treatment conditions (different kinetic regimes) can allow to determine all the parameters one by one in each specific experimental conditions in which some of the parameters have a negligible influence upon the redistribution profile. For example, Fig. 8 shows the influence of B clusters upon P diffusion in polycrystalline Si [11]. Initially, the P distribution in the poly-Si film is almost homogeneous, however, during annealing P atoms diffuse toward B clusters against the P concentration gradient. P atoms gather underneath the Gaussian distribution of B clusters, and form also a Gaussian distribution. This P uphill diffusion can be simulated by taking into account the chemical interactions between P and B atoms, expressing the P chemical potential as a function of the B concentration. Considering that the system is a regular ternary solution containing Si, B and P atoms, and that $X_{Si} \to 1$ and $(1 + X_B) \sim 1$ in our case, the chemical potential of the P atoms (μ_P) can be expressed as:

$$\mu_P \approx kT\ln X_P + V^{SiP} + X_B\left(V^{PB} - V^{BSi}\right) = kT\ln X_P + V^{SiP} + X_B\Delta V\ . \quad (6)$$

$$\text{with } V^{ij} = \varepsilon^{ij} - \frac{1}{2}\left(\varepsilon^{ii} + \varepsilon^{jj}\right). \quad (7)$$

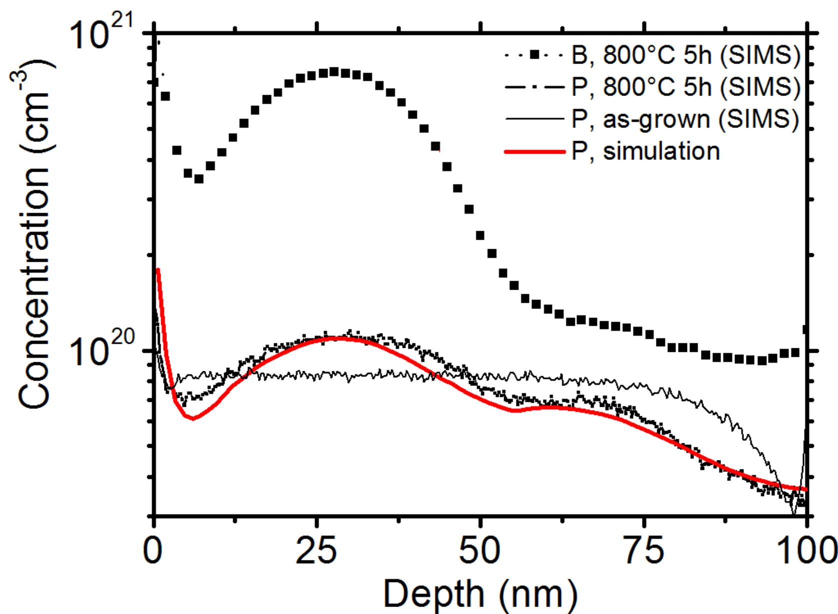

Fig. 8. SIMS profiles of B (solid squares) and P (doted line) measured in the same sample after annealing at 800°C for 5 hours, compared to the initial P profile measured by SIMS (thin solid line). The P profile simulated with $D_g = 3.38\times10^{-17}$ cm^2 s^{-1}, $D_{gb} = 1.1\times10^{-13}$ cm^2 s^{-1} and $\Delta V \sim 6.94$ eV is also presented in red thick solid line.

X_i is the atomic ratio of the element i in the solution, and $\varepsilon^{ij} < 0$ is the pair interaction energy of the two elements *i* and *j*. V^{ij} describes the nature of the interactions between the elements *i* and *j*: if $V^{ij} > 0$ the interactions are repulsive, if $V^{ij} < 0$ the interactions are attractive. The first term in Eq. (6) corresponds to the usual diffusion driving force in the Fick equations [2], while the two other terms can be used for the definition of an extra driving force using the Nernst Einstein equation [2]. The flux of P atoms is then expressed as:

$$J = -D_P \nabla C_P - C_P D_P \frac{\Delta V}{kT} \nabla X_B \text{ with } \Delta V = \varepsilon^{PB} - \varepsilon^{BSi} + \frac{1}{2}\left(\varepsilon^{SiSi} - \varepsilon^{PP}\right). \quad (8)$$

C_P is the P concentration and D_P is the diffusion coefficient of P. Eq. (8) can be used to simulate P diffusion in the poly-Si matrix during annealing [11]. The simulation presented in Fig. 8 at 800°C was performed in two dimensions following the Fisher model [18], and considering a constant B distribution as observed experimentally (solid squares in Fig. 8). The simulation model contains 5 parameters: i) the lateral size of the grains (l), ii) the lateral size of the GBs (δ), iii) the P diffusion coefficient in the Si grains (D_g), iv) the P diffusion coefficient in GBs (D_{gb}), and v) the parameter ΔV that is related to the P-B interactions. These parameters cannot be extracted simultaneously from the experimental SIMS profiles. However, several of them are actually known from measurements in the studied samples (microstructure) or from the literature. Thus, four parameters over five could be set in the simulations presented in Fig. 8: l = 50 nm, δ = 0.5 nm [24], $D_g = 3.38\times10^{-17}$ cm^2 s^{-1} [2], and $D_{gb} = 1.1\times10^{-13}$ cm^2 s^{-1} [23]; allowing for the measurement of the fifth parameter ΔV. We found $\Delta V \sim -6.94 \pm 0.2$ eV at 800°C. Furthermore, thanks to this model several diffusion conditions could be investigated. For example, Eq. (8) could be used to describe diffusion only in the grains, using the conventional Fick equation in GBs, and vice versa. The case of diffusion in grains only or in GBs only could also be investigated, and the effect of different combinations of diffusion coefficient values was studied. These investigations shown that, in our experimental conditions, P must diffuse in the grains in order to fit the experimental profile, leading to the conclusion that P diffusion uses the type *B* kinetics regime at 800°C in poly-Si. Furthermore, if the P-B interaction is taken into account in GBs only and not in grains, there is not enough matter in the GBs in order to fit the experimental profile, meaning that the chemical attraction between P and B atoms has to be effective both in the grains and in the GBs to match the experimental results.

3D simulations. In nanocrystalline films, the contribution of TJs to the effective diffusion of impurities through the layer can be large, and consequently TJ diffusion coefficients need to be measured in order to predict nanocrystalline materials aging. To this aim, we proposed to use a similar method as described before, but using a 3D geometry able to consider grain, GB, and TJ diffusion paths [9, 25]. Contrasting with the 2D simulations, the diffusion coefficients in the three different paths cannot be measured simultaneously using 3D simulations. However, if the GB diffusion coefficient is known, then the diffusion coefficients in grains and TJs can be measured simultaneously. In order to minimize the calculation time, the 3D geometry of the model needs to be as reduced as possible using the different symmetries of the structure. Figure 9a presents the top view of the reduced 3D geometry used to model a polycrystalline layer made of squared grains in the plan xy. Figure 9b presents the 3D geometry with a Gaussian atom distribution before annealing, and the 3D result after annealing simulation. In this case, the grain width is 40 nm and the film thickness is 500 nm.

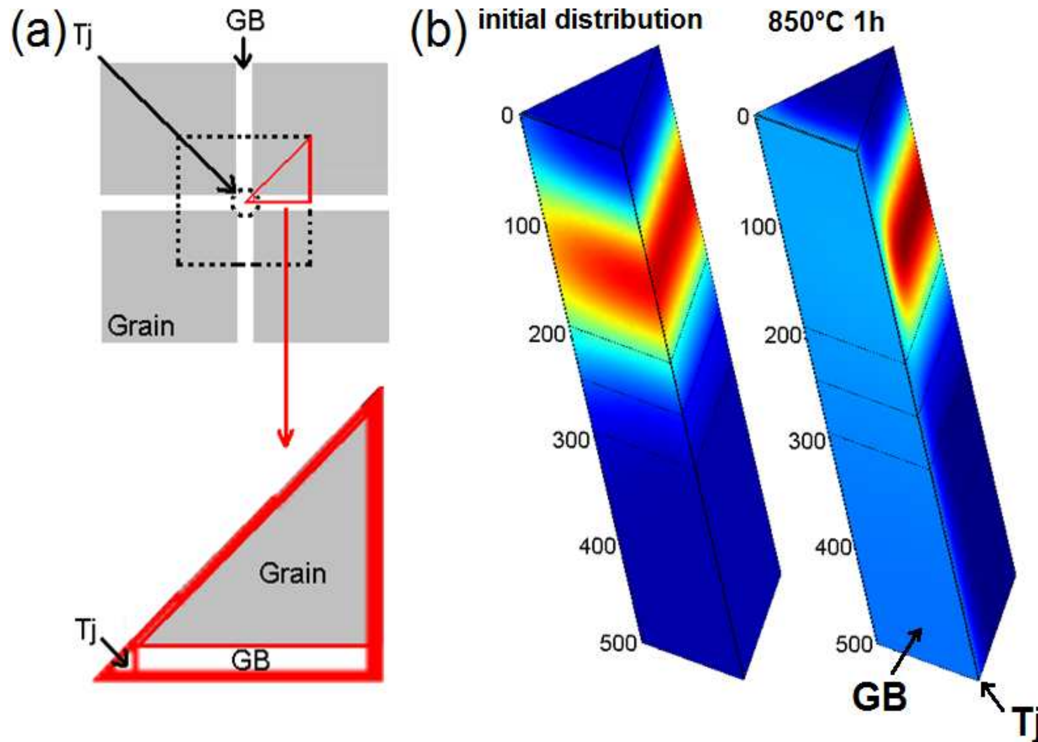

Fig. 9. Geometry used for 3D simulations taking into account lattice, GB, and TJ diffusion paths: (a) top view, and (b) 3D view before and after annealing simulation.

Diffusion in nanocrystalline materials has been shown in several examples to be faster than in microcrystalline materials [26-27]. However, the reason for this diffusion enhancement is still under debate, and may depend upon sample nature (metals, semiconductors, pure elements or alloys…) as well as sample fabrication process (residual stress, microstructure…). The Si-Ge system appears to be an ideal system to investigate diffusion in nanocrystalline layers. Si nanocrystalline layers can be produced by chemical vapour deposition with a high purity and no residual stress. Furthermore, Ge and Si are totally miscible, Ge segregation in Si GBs is negligible, and Ge uses the same vacancy mechanism to diffuse in Si up to 1000°C.

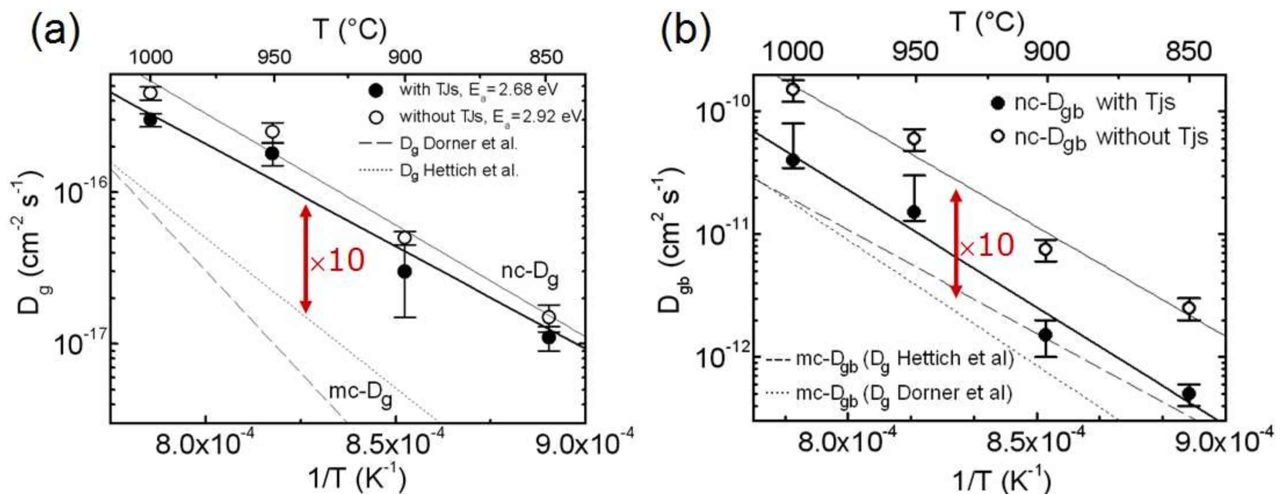

Fig. 10. Comparison between Ge diffusion in nano-crystalline poly-Si measured using 2D simulations without TJs (open circles) or 3D simulations with a constant diffusion coefficient in TJs (solid circles): (a) Ge lattice diffusion in 40 nm-wide Si grains compared with Ge lattice diffusion in mono-Si (broken lines), and (b) Ge diffusion in nano-GBs compared with Ge diffusion in micro-GBs (broken lines).

Figure 10 presents the Ge diffusion coefficients measured versus temperature in a same polycrystalline Si layer made of 40 nm-wide grains using either a 2D model without considering TJs (open circles) or using a 3D model with TJs (solid circles) [25, 28]. For the 3D simulations, the TJ diffusion coefficient was kept constant and equal to 10^{-9} cm^2 s^{-1}, which is about 10^3 times lower than the Si surface diffusion coefficient in our temperature range. The coefficients are compared with Ge lattice diffusion in Si bulk (broken lines [29-30]) and Ge diffusion in Si micro-GBs [28]. With or without considering TJ diffusion, the diffusion coefficients measured in the nano-grains are found to be about one order of magnitude faster than in the Si single crystal (Fig. 10a). About the same diffusion coefficient is found in the two cases with nano-D_g = 1.97×10^{-4} exp(−2.92eV/kT) cm^2 s^{-1} in the grains.

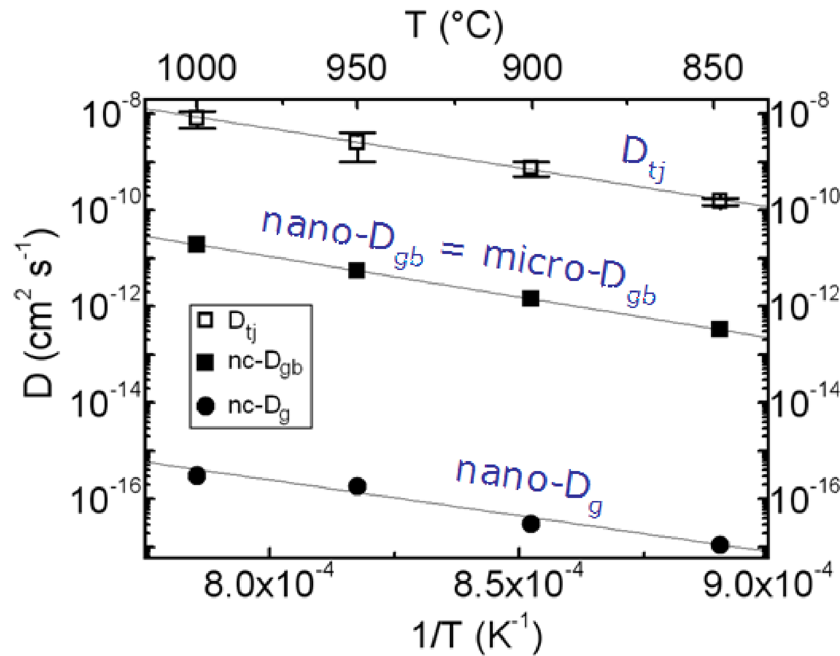

Fig. 11. Ge difusion coefficients mesured in a nanocrystalline poly-Si layer using 3D simulations.

With the 2D model, the nano-GB diffusion coefficients are found to be about 10 times higher than the micro-GB coefficients. With the 3D geometry, despite that the TJ diffusion coefficient is kept constant for all the different temperatures, one can note that the nano-GB coefficients are found to be close to the values of Ge diffusion in micro-GBs, which is in agreement with experimental measurements performed in different materials, showing that diffusion in nano-GBs is actually similar to diffusion in micro-GBs [31]. Consequently, using a 2D geometry, the GB diffusion in nanocrystalline layers can be overestimated due to the contribution of TJ diffusion, depending on the nano-grain size. Figure 11 presents the Ge diffusion coefficients measured in the Si polycrystalline layer made of 40 nm-wide grains using the 3D Fisher geometry, and imposing in GBs the diffusion coefficient measured in micro-GBs. We found D_{Tj} = 5.72 × 10^4 exp(−3.24 eV/kT) cm^2 s^{-1} in TJs. Consequently, these results show that enhanced Ge diffusion in nanocrystalline Si is due to the combination of faster lattice diffusion in nano-grains and fast diffusion in TJs [25]. Using the 3D Fisher model, the lattice diffusion and TJ diffusion coefficients were measured simultaneously thanks to the knowledge of the GB diffusion coefficient. Figure 12 presents a summary concerning Ge diffusivity in Si. The Ge diffusion coefficient on the Si(111) surface is from ref. [32], and the lattice diffusion of Ge in monocrystalline Si is from ref. [29], the other measurements in 40 nm-wide Si crystal, Si GBs and TJs are the extrapolation of the measurements performed using 3D FES. It is interesting to note that at high temperature the enhanced Ge lattice diffusion coefficient found in Si nano-grains converges to the Ge lattice diffusion coefficient measured in monocrystalline Si. Furthermore, the TJ diffusion coefficient is always lower than the surface diffusion coefficient, and at high temperature these two coefficients are also found to be very close.

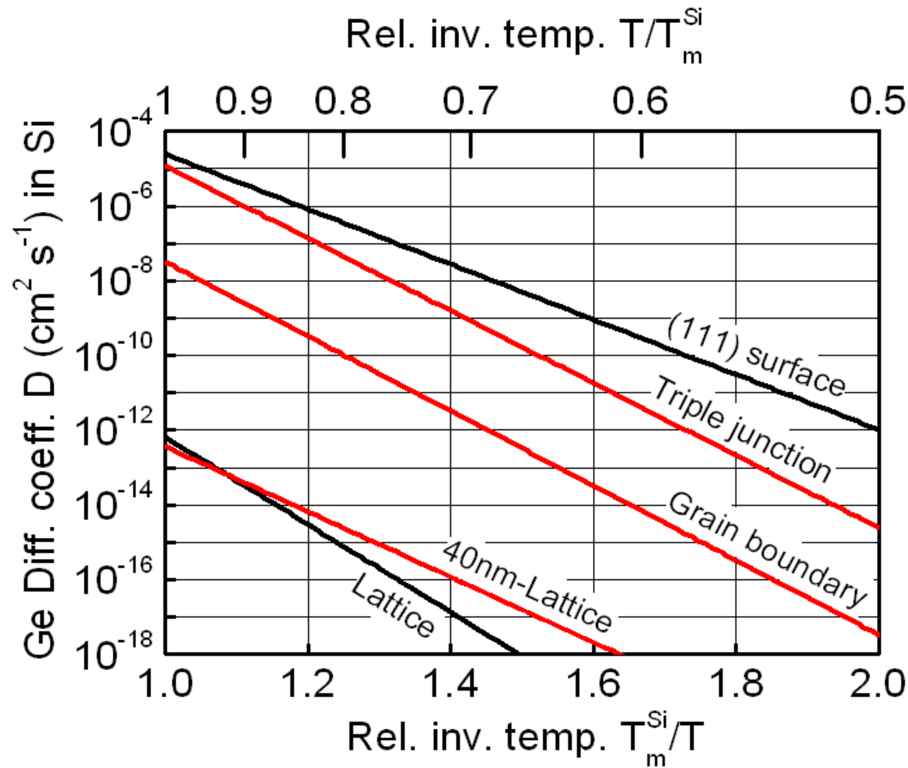

Fig. 12. Ge diffusion in Si via different diffusion paths.

Atom Probe Tomography measurements

In the previous sections we showed that 2D or 3D FES combined with usual 1D experimental concentration measurements can allow diffusion measurements in grains, GBs, and TJs of polycrystals. This method relies on the use of a model that can correctly represent the microstructure of the sample, and sometimes requires the knowledge of some of the diffusion coefficients in the different diffusion paths in the sample (lattice, GBs, TJs). Consequently, the measurements of diffusion coefficients in GBs and TJs, especially in nanocrystalline samples, are indirect. Diffusion coefficient in grains, GBs, and TJs of polycrystals could be obtained via more direct methods if impurity concentration could be accurately measured in grains, GBs, and TJs. This suggests the use of an experimental tool allowing chemical analyses at the atomic scale, since GB width is usually about 0.5 nm. Thus, APT microscopy seems to be the only tool available today providing chemical analyses in the 3 space dimensions (x, y, z) at this requested scale [33-34]. APT is a destructive technique that allows i) the electric field evaporation of the atoms composing the sample (shaped as a needle) at very low temperature (20 to 80 K) and ii) the 3D “reconstruction” of the volume of the sample at the atomic scale [35]. Using APT, 1D, 2D and 3D atomic distributions of a given atom in a sample can be obtained.

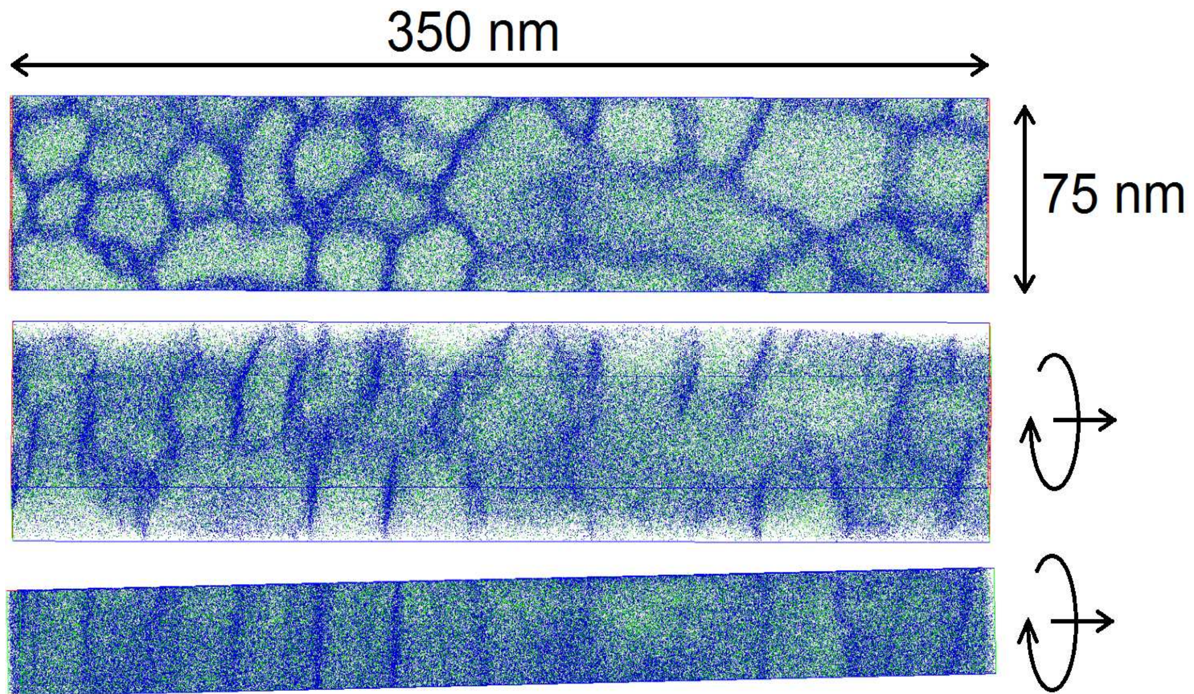

Fig. 13. 3D volume of a polycrystalline $Ni_2Si(Pt)$ layer obtained by APT microscopy. Each point is an atom, gray, green and blue points corresponding to Si, Ni and Pt atoms, respectively. The three images correspond to the same volume observed at different angles due to a 90° rotation (first in top view and last in side view).

For example, Fig. 13 presents APT measurements performed on a polycrystalline $Ni_2Si(Pt)$ layer. This layer was obtained by reacting Ni(5%Pt) with Si. The sample was prepared by focused ion beam lift-out with the tip-shaped sample oriented in the direction parallel to the film plane (cross-sectional preparation). Only the $Ni_2Si(Pt)$ layer is shown. The accumulation of Pt atoms in the grain boundaries is clearly observed, revealing the shape and the size of the Ni_2Si grains.

Grain boundaries. APT is an essential tool to obtain three dimensional atomic distributions in materials. In addition, it allows direct measurement of the concentrations without requiring corrections, unlike more conventional techniques as SIMS [36]. It also has a better spatial resolution than SIMS [37] that is affected by collisional mixing effects [36]. It is, thus, particularly adapted to the chemical characterization of GBs [38-42]. However, APT does have limitations too and it is important to understand how these limitations can affect the measured data in order to ensure a correct interpretation of the results. One point of great importance for the characterization by APT of grain boundaries, or interfaces in general, is the spatial resolution anisotropy. This anisotropy arises from the fact that the resolution along the direction of analysis (z), and the lateral resolution (xy plane – i.e. perpendicular to the direction of analysis) depend on different physical phenomena. In a reconstructed volume, atom positions along the z axis depend solely on the atom ebvaporation order, while the resolution in the xy plane depends on the trajectory of the evaporated ions, which can be affected by irregularities on the tip surface. Indeed, when different phases with different evaporation fields are present at the surface of the sample, local changes in the surface curvature can arise and cause local magnification effects [43-44]. This has to be taken into account when characterizing interfaces, because interfaces themselves can have a different field of evaporation [45]. It is very important for heterophase interfaces, where the differences in magnification between the two phases can sometimes cause trajectory overlaps [44, 46] and deteriorate the lateral spatial resolution at the interface. In addition to these effects, surface diffusion can also have undesirable effects upon lateral resolution [47].

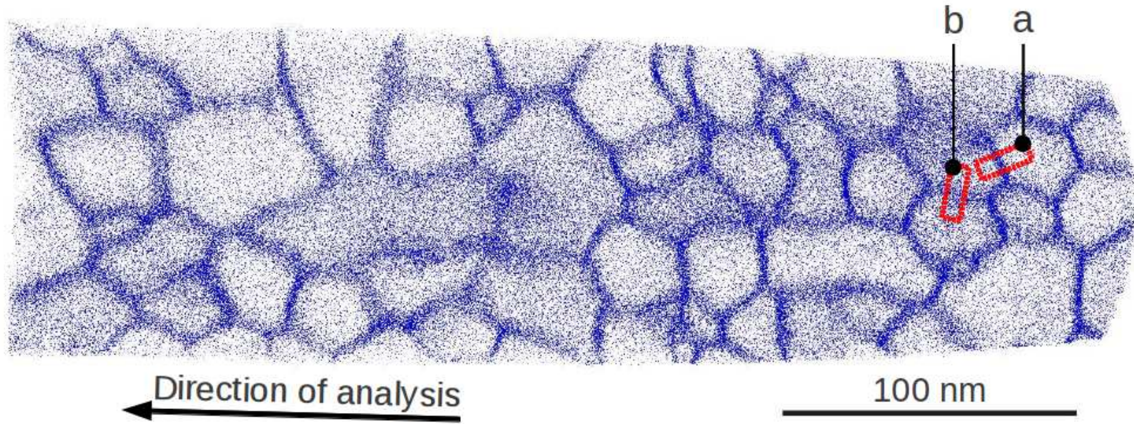

Fig. 14. Normal projection of the 3D reconstruction of a $Ni_2Si(Pt)$ thin film. Only the Pt atoms are shown for clarity. The red boxes show the grain boundaries for which the profiles are shown in Fig. 15a and b.

These effects on the spatial resolution can be observed experimentally. For example, the total analyzed volume of the $Ni_2Si(Pt)$ film presented in Fig. 13 is shown in Fig. 14. Only the Pt atoms are shown for clarity. To study how the spatial resolution affects the observed Pt distribution at GBs, concentration profiles were measured across 79 of the observed GBs. The profiles are measured using boxes of 5×20 nm² in cross section that are placed perpendicularly to the GBs. Care was taken to avoid overlaps between different GBs or with triple junctions. The left profile (Fig. 15a) is measured across a GB that forms an angle $\theta = 70.3°$ with the direction of analysis and the right profile (Fig. 15b) corresponds to a GB oriented with an angle $\theta = 2.0°$. The width of the GB is smaller when the GB forms a high angle with the direction of analysis. It must be noted that the maximum concentration is smaller for the wide GB, showing that the broadening of the GB can not be due to local magnification effects only, because local magnification affects the measured density and leaves the concentrations unchanged. This is evidence that atom mixing occurs at the interface, thereby affecting the spatial resolution.

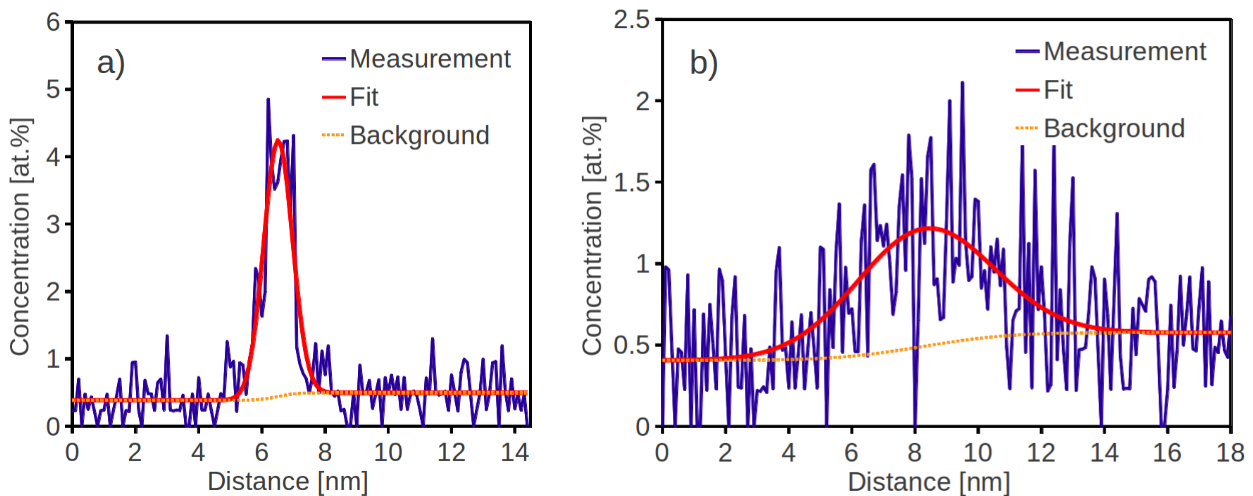

Fig. 15. Pt concentration profiles measured across two grain boundaries that form an angle (a) $\theta = 69.0°$ and (b) $\theta = 2.0°$ with the direction of analysis. The concentration profiles are fitted with Gaussian functions, taking into account the differences in concentrations between the two grains.

In order to verify this effect on GB width, the widths of the GBs are measured using a fit of the concentration profile using a Gaussian distribution. Slightly different Pt concentrations were sometimes measured in two adjacent grains. To account for these differences in concentrations, the profiles are fitted using two functions: the concentration in the grain boundary is fitted using the distribution $G(x)$, while the concentrations in both grains are fitted using a background function $E(x)$ that is the convolution of $G(x)$, and a step function describing the concentration in both grains:

$$f(x) = G(x) + E(x) \tag{9}$$

$$f(x) = C_{\max} \exp\left(\frac{-(x-\mu)^2}{2\sigma^2}\right) + \left[erf\left(\frac{x-\mu}{\sqrt{2}\sigma}\right)+1\right]\left(\frac{C_2 - C_1}{2}\right) + C_1 \tag{10}$$

where C_{max} is the maximum value of $G(x)$, μ is the position of the interface, σ is the standard deviation of the Gaussian distribution, erf(x) is the error function, and C_1 and C_2 are the concentrations on the left and the right side of the profile, respectively. The full width at half maximum (FWHM) of the Gaussian distribution is then given by the relation $FWHM = 2\sqrt{2\ln(2)}\sigma$.
The orientations of the different GBs are measured using two different definitions (Fig. 16). In one hand, the orientation is simply defined as the angle θ between the GB and the direction of analysis $\vec{u}$, and in another hand, it is defined as the angle α between the GB and the normal to the tip surface $\vec{v}$ at the moment which the atoms in the GB were being evaporated. This direction depends on the position of the GB at the tip surface, but also on the tip's radius of curvature when the GB was being evaporated. Independently of the definition used, it is clear in Fig. 17 that the smaller the angle, the larger the FWHM.

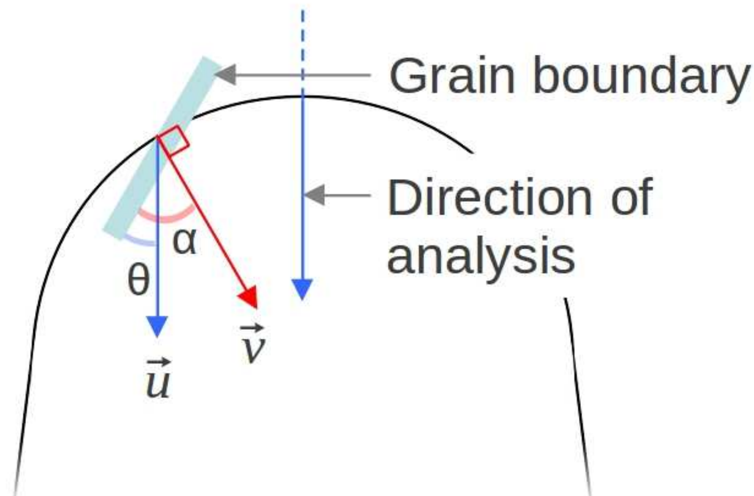

Fig. 16. Schematic of the two angles used to characterize the orientation of the GB. θ is the angle between the GB and the direction of analysis $\vec{u}$, and α the angle between the GB and the normal to the tip surface $\vec{v}$.

It is obvious that the spatial resolution is generally poorer in the lateral direction. However, the scattering of the data in Fig. 17 is reduced when the angle α with respect to the normal to the tip surface is used (Fig. 17b), showing that the use of the angle α is more relevant to account for the real mechanisms involved in the spatial resolution. Indeed, after data acquisition, the reconstruction procedure consists in the back-projection of the atoms from where they hit the detector, to a

hypothetical hemispherical surface that represents the tip [13, 48]. Thus, the error on the position of an ion that hit the detector (due to local magnification effects, surface diffusion...etc) eventually causes errors in the position of the atom within the surface of that hemispherical surface only, and not in the *xy* plane. Therefore, the best resolution normal to a GB is obtained when that GB is parallel to the tip surface, and not necessarily to the *xy* plane. This point should be taken into account when trying to optimize the resolution normal to a GB, or to an interface in general. In the present case, when the best resolution is obtained, the FWHM is equal to 1 nm, which is close the experimental value of GB width measured by TEM (0.5-1 nm), or obtained comparing GB diffusion experiments in *B* and *C* kinetic regimes (0.5 nm), and the averaged value usually used (0.5 nm) [1]. Assuming that the spatial resolution along the tip surface is described by a Gaussian distribution of standard deviation ε, the apparent GB width is given by:

$$\delta' = \sqrt{\delta^2 + (\varepsilon \cos(\alpha))^2} \qquad (11)$$

where δ is the real GB width. The dotted line in Fig. 17b corresponds to δ' calculated with $\delta = 1$ nm and $\varepsilon = 3$ and 7 nm. The scattering of the data for low angles is likely to be due to local magnification effects that were observed from one grain to another, causing density changes of ± 50% of the average density (not shown here), which corresponds to the magnitude of the scattering of the values of δ'.

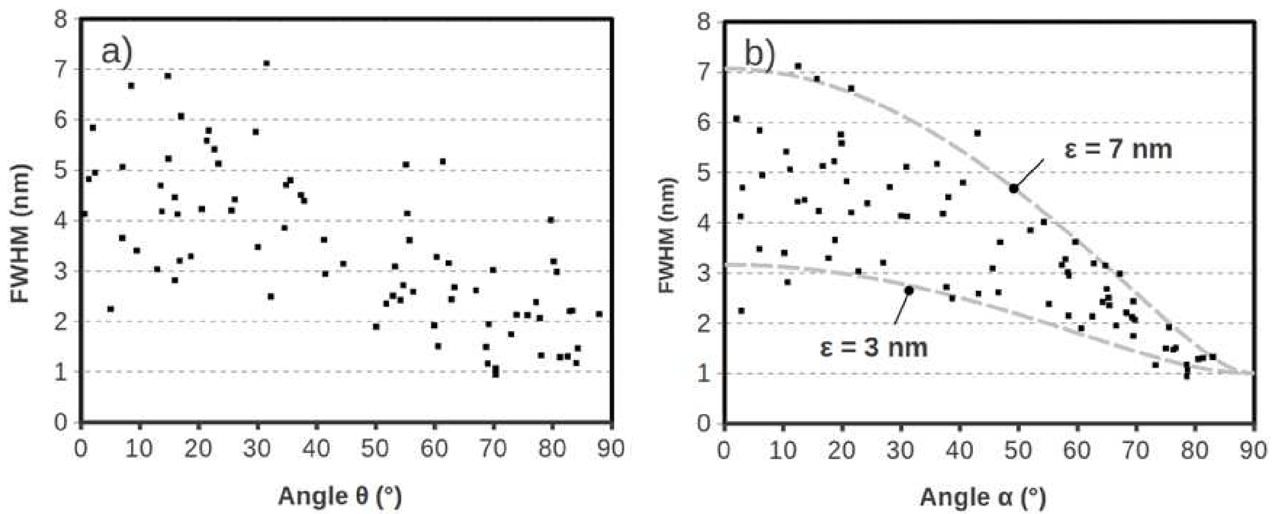

Fig. 17. Measured GB width with respect to (a) the angle θ between the GB and the direction of analysis and (b) the angle α between the GB and the normal to the tip surface. The dashed lines show the GB width predicted using a lateral spatial resolution of 3 and 7 nm.

In summary, the spatial resolution of the APT is not isotropic; the resolution normal to a GB will depend on its orientation and its position on the tip surface during the evaporation. In general, the spatial resolution in a GB is poorer if the GB orientation is parallel to the analysis direction (small θ and α angles). Thus, if the diffusion source is on the surface of the analyzed material, analyzing the material by APT in the top-down direction (i.e. perpendicular to the surface) will have little or no effect on the resolution normal to the surface. In this case, for a 1D concentration profile measured perpendicular to the surface over a representative volume, the measured concentrations will not be affected by the spatial resolution nor local magnification effects, which affect only the measured density. However, this will have consequences when studying the concentration profile across GBs or when trying to measure the concentration in a GB. The spatial resolution is poorer along the tip surface, thus GBs that are perpendicular to the tip surface can be strongly broaden. A poor spatial resolution will cause atoms that are accumulated at the GB to be detected around the GB. If a diffusion field exists around the GB, it might then overlap with these atoms which could lead to

errors in the estimation of the bulk diffusion coefficient. In a worse case, the atoms around the GB might be interpreted as a real diffusion field, leading to the conclusion that the diffusion in the volume is significant, when the diffusion regime might actually be of type *C*. Loss in the resolution normal to the GB will also reduce the measured maximum concentration of the segregating specie, leading to errors in the measured segregation factor. It can be noted that it will not affect the value of the Gibbs's interfacial excess [35, 49] which gives the density of atoms per unit area independently of the resolution normal to the GB. However, as we have shown, when a GB is oriented parallel to the tip surface, the spatial resolution is good enough so that the contributions from the GB and the bulk of the grain can be clearly separated, and concentrations can be measured more accurately. This shows that, when accurate local concentrations are needed, analysis perpendicular to the GBs of interest are preferable, or, for example, analysis parallel to the plane of the film in the case of columnar grains.

Diffusion profiles. Fig. 18 shows schematically a sample that has been analyzed by APT. A 40 nm-thick Ni layer was deposited on a Si substrate, and capped with a 5 nm-thick Pt layer. After annealing (~250°C) Ni has reacted with Si to form the compound Ni_2Si that is polycrystalline. Because of the limited amount of Ni, eventually the poly-Ni_2Si layer stopped growing and its thickness stayed constant during the rest of the annealing. Pt atoms could be incorporated in the Ni_2Si film during Ni-Si reaction, but once Ni_2Si stopped growing, Pt atoms could diffuse through the Ni_2Si to reach the substrate, and Si atoms could diffuse through Ni_2Si to the Pt source layer.

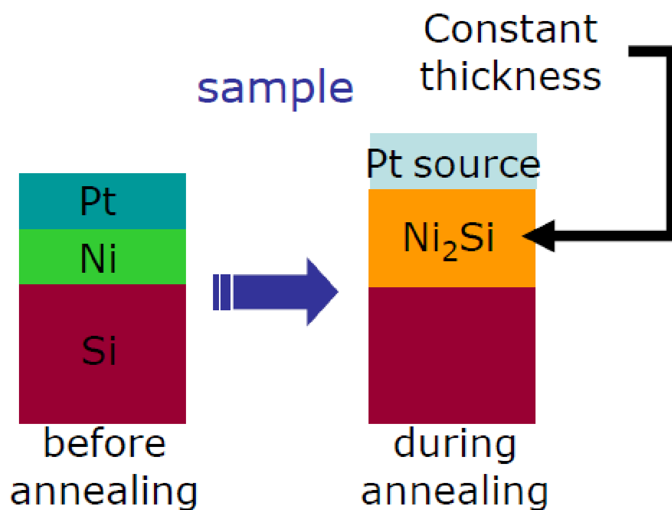

Fig. 18. Schematic of the sample: before annealing and after reaction between the Pt and Ni layers with the Si substrate.

Figure 19 presents APT measurements performed in this sample. The direction of analysis is perpendicular to the film surface. Fig. 19a corresponds to a 2D mapping of the Pt concentration at a given depth in the poly-Ni_2Si layer. We can observe that Pt concentration is higher in GBs than in grains, and that the Pt content of TJs is higher than the Pt content of GBs. The grains have a rectangular shape, and correspond to the lower height with a blue color (< 1 at. %). The GBs are forming lines between grains with an intermediate height and a lighter blue color (3-4 at. %), and the triple junctions correspond to the intersections of the GBs with a color between yellow and red (5-6 at. %), similar to the model presented in Fig. 9.

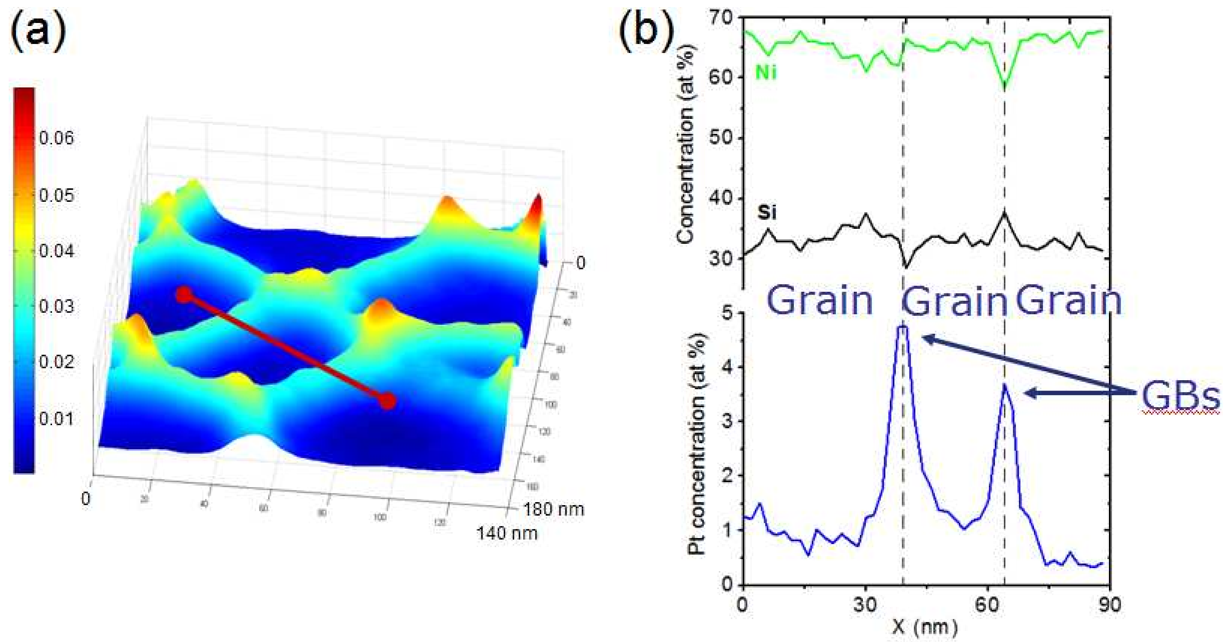

Fig. 19. APT measurements in a polycrystalline $Ni_2Si(Pt)$ layer: (a) 2D distribution of Pt atoms at a given depth in the layer, and (b) concentration profiles measured along the red line in (a).

Figure 19b presents 1D profiles measured along the red line in Fig. 19a. As expected, Ni and Si concentrations are quite constant and correspond to the stœchiometry of the Ni_2Si compound. In contrast, the Pt distribution is not homogeneous in grains and GBs, with a concentration close to 1 at. % in the grains, and between 3.5 and 5 at. % in GBs. These variations are in agreement with a faster Pt diffusion in GBs than in grains. Thanks to the APT profile through grains and GBs, the ratio between atom concentration in grains and in GBs can be determined, which can be very useful in order to study atom segregation in GBs. In our case, we measured an averaged ratio $C_{gb}/C_g \sim 8$ for Pt atoms. Figure 20a presents the top view of the 3D distribution of Pt atom in the Ni_2Si layer. Each blue point is a Pt atom. Here also it is clear that the concentration of Pt atoms is greater in GBs than in grains. The shape and the size of the grains are also easily determined from the APT data. The cylinder presented in this figure corresponds to the volume in which the 1D profiles presented in Fig. 20b have been calculated. As shown in the Fig. 20a, the cylinder has been aligned along a GB, passing through i) the grain #1, ii) a first TJ, iii) the GB, iv) another TJ, and finally v) the grain #2. The Pt concentration profile presented in Fig. 20b shows that at a same depth, the Pt concentration is higher in TJs than in GBs. This is in agreement with a faster diffusion in TJs than in GBs as it has been previously concluded using analytical models [49]. Thanks to this profile, the ratio between the impurity concentration in grains or GBs and TJs can be determined. We found in our case the averaged ratios $C_{Tj}/C_{gb} \sim 1.82$ and $C_{Tj}/C_g \sim 7.6$. It is interesting to note that in our sample $C_{gb}/C_g \sim C_{Tj}/C_g$.

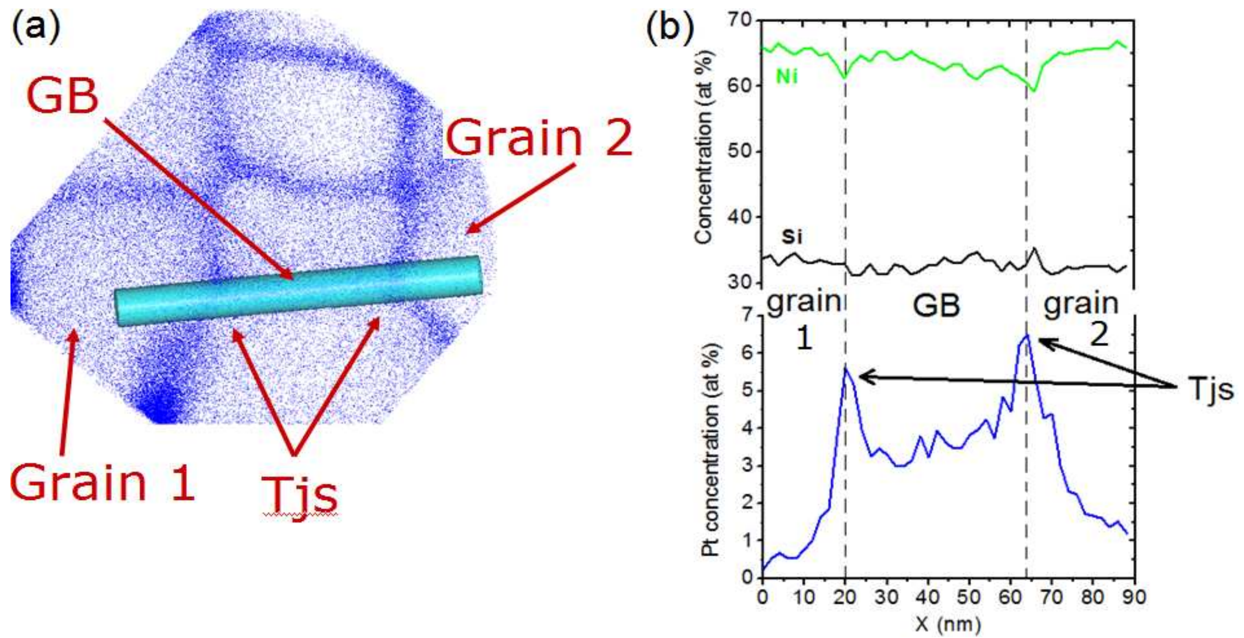

Fig. 20. APT measurements in a polycrystalline $Ni_2Si(Pt)$ layer: (a) top view of the 3D distribution of Pt atoms, and (b) concentration profiles measured in the 3D cylinder presented in (a).

Figure 21 presents the 1D concentration profiles of Pt through the Ni_2Si layer in a selected grain (solid line), a selected GB (solid squares), and a selected TJ (open squares). As previously mentioned, the poly-$Ni_2Si(Pt)$ layer results from the reaction of a Pt/Ni bilayer with a Si(001) substrate. Thus, the Pt concentration in the different part of the sample can result from both incorporation during Ni-Si reaction and diffusion after this reaction. For example, due to the low annealing temperature, the Pt profile in the grain can be interpreted as resulting from Pt incorporation during reaction. In the GB the Pt concentration forms a small gradient, but the Pt concentration is flat in the TJ, which is consistent with a faster TJ diffusion compared to GB diffusion.

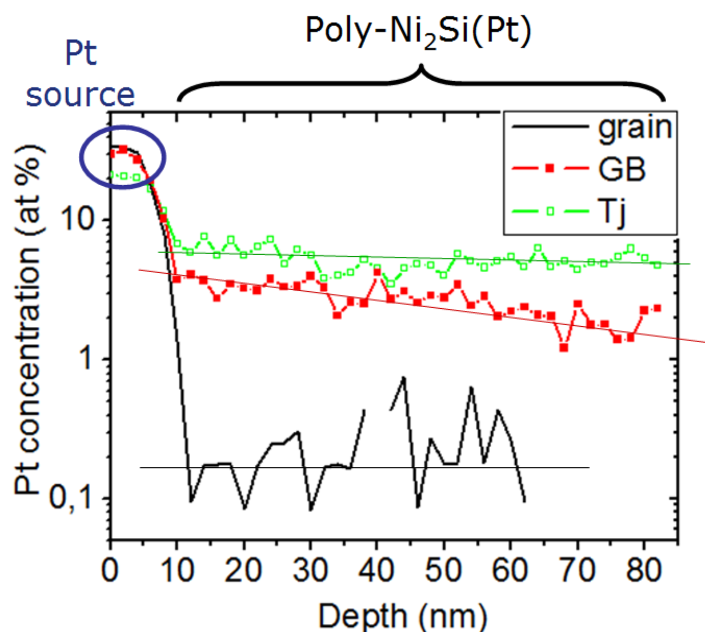

Fig. 21. Pt concentration profiles measured in a single grain (solid line), a single GB (solid squares), and a single TJ (open squares) in a polycrystalline $Ni_2Si(Pt)$ layer.

In type *C* controlled diffusion experiments, these types of profiles compared with FES or diffusion analytical solutions should permit to measure in polycrystals the diffusion coefficients in GBs and TJs independently. However, as it was shown previously, both the dimension of the GBs and the concentration can be affected by APT artifacts. In the future, it will be important to imagine some procedures ensuring that their effects are negligible on the diffusion coefficient measurements. Furthermore, APT measurements are extremely local, leading to a low statistic. For example, GB diffusion may vary with GB orientation, thus, the diffusion coefficient measured in a specific GB may not correspond to the diffusion coefficient averaged over many GBs, as measured using more global techniques as SIMS. A comparison between coefficient measurements obtained in a same sample either using 3D FES and 1D SIMS profiles (important statistic) or using 3D FES and APT measurements should provide information about the homogeneity of the sample.

Summary

Original methods allowing for the measurement of diffusion coefficients in polycrystalline and nanocrystalline layers have been presented and discussed. The first method consists of comparing usual 1D concentration profiles measured before and after sample annealing to 2D or 3D simulations in order to extract the averaged diffusion coefficients in grains, GBs, and TJs. For example, thanks to this method, it has been shown that Ge diffusion in Si nano-grains is faster than in Si monocrystal, Ge diffusion in Si nano-GBs is similar to diffusion in mico-GBs, and Ge diffusion in Si TJs is faster than in GBs. The second method uses the comparison between simulations and APT measurements. APT can promote direct measurement of diffusion coefficients as well as segregation coefficients in GBs and TJs, since it allows the impurity concentration in these defects to be measured at the atomic scale. Of course, as for any experimental technique, the results can be affected by experimental artifacts, as those linked to the APT spatial resolution in our case. This is why it will be necessary to confirm the validity of diffusion coefficients measured by APT, using comparisons with the usual techniques. Even so, it is interesting to note that when the analysis conditions are optimized, spatial resolution close to the GB width itself can be obtained.

References

[1] H. Mehrer: *Diffusion in Solids* (Springer-Verlag, Berlin Heidelberg, 2007).

[2] P. Pichler: *Intrinsic Point Defects, Impurities, and their Diffusion in Silicon* (Springer-Verlag/Wien New York, Austria, 2004).

[3] A. Portavoce, P. Gas, I. Berbezier, A. Ronda, J. S. Christensen, A. Yu. Kuznetsov, and B. G. Svensson: Phys. Rev. B Vol. 69 (2004), p. 155415.

[4] N. Rodriguez, A. Portavoce, J. Delalleau, C. Grosjean, V. Serradeil, and C. Girardeaux: Thin Solid Films Vol. 518 (2010), p. 5022.

[5] P. Pichler, A. Burenkov, J. Lorenz, C. Kampen and L. Frey: Thin Solid Films Vol. 518 (2010), p. 2478.

[6] E.M. Bazizi, A. Pakfar, P.F. Fazzini, F. Cristiano, C. Tavernier, A. Claverie, N. Zographos, C. Zechner, and E. Scheid: Thin Solid Films Vol. 518 (2010), p. 2427.

[7] J.A. Sethian and J. Wilkening: J. Comput. Phys. Vol. 193 (2003), p. 275.

[8] M. Pernach and M. Pietrzyk: Comput. Mater. Sci. Vol. 44 (2008), p. 783.

[9] A. Portavoce, I. Blum, L. Chow, J. Bernardini, and D. Mangelinck: Defect and Diffusion Forum Vols. 309-310 (2011), p. 63.

[10] A. Portavoce, R. Simola, D. Mangelinck, J. Bernardini1, and P. Fornara: Diffusion and Defect Data Vol. 264 (2007), p. 33.

[11] A. Portavoce, D. Mangelinck, R. Simola, R. Daineche, and J. Bernardini: Defect and Diffusion Forum Vols. 289-292 (2009), p. 329.

[12] A. Kikuchi and S. Sugaki: J. Appl. Phys. Vol. 53 (1982), p. 3690.

[13] M. Qin, V. M. C. Poon, and S. C. H. Ho: J. Electrochem. Soc. Vol. 148 (2011), p. G271.

[14] J. Kedzierski, D. Boyd, P. Ronsheim, S. Zafar, J. Newbury, J. Ott, C. Cabral, Jr., M. Ieong, and W. Haensch, in: IEEE International Electron Devices Meeting - IEDM 2003, South Lake Tahoe, USA, 2003 (Electron Devices Society, New York, 2003).

[15] I. Blum, A. Portavoce, D. Mangelinck, R. Daineche, K. Hoummada, J.L. Lábár, V. Carron, and C. Perrin: J. Appl. Phys. Vol. 104 (2008), p. 114312.

[16] I. Blum, A. Portavoce, D. Mangelinck, R. Daineche, K. Hoummada, J.L. Lábár, V. Carron, and J. Bernardini: Microelectronic Engineering Vol. 87 (2010), p. 263.

[17] F. Nemouchi, D. Mangelinck, C. Bergman, P. Gas, and U. Smith: Appl. Phys. Lett. Vol. 86 (2005), p. 041903.

[18] J. C. Fisher: J. Appl. Phys. Vol. 22 (1951), p. 74.

[19] C. E. Allen, D. L. Beke, H. Bracht, C. M. Bruff, M. B. Dutt, G. Erdélyi, P. Gas, F. M. d'Heurle, G. E. Murch, E. G. Seebauer, B. L. Sharma, and N. A. Stolwijk, in: *Diffusion in Semiconductors and Non-Metallic Solids*, Landolt-Börnstein-Numerical Data and Functional Relationships in Science and Technology, edited by D. Beke (Springer-Verlag, Berlin, 1998), Vol. 33.

[20] H. Bakker, H. P. Bonzel, C. M. Bruff, M. A. Dayananda, W. Gust, J. Horváth, I. Kaur, G. V. Kidson, A. D. Le Claire, H. Mehrer, G. E. Murch, G. Neumann, N. Stolica, N. A. Stolwijk, in: *Diffusion in Solid Metals and Alloys*, Landolt-Börnstein-Numerical Data and Functional Relationships in Science and Technology, edited by H. Mehrer (Springer-Verlag, Berlin, 1990), Vol. 26.

[21] Y. Mishin, C. Herzig, J. Bernardini, and W. Gust: International Mat. Rev. Vol. 42 (1997), p. 155.

[22] P. M. Farley, P. B. Griffin, and J. D. Plummer: Rev. of Mod. Phys, Vol. 61 (1989), p. 316.

[23] K. Sakamoto, K. Nishi, T. Yamaji, T. Miyoshi, and S. Ushio: J. Electrochem. Soc. Vol. 132 (1985), p. 2457.

[24] L. G. Harrison: Trans. Faraday Soc. Vol. 57 (1961), p. 1191.

[25] A. Portavoce, L. Chow, and J. Bernardini: Appl. Phys. Lett. Vol. 96 (2010), p. 214102.

[26] Y. Chen and C. A. Schuh: Scr. Mater. Vol. 57 (2007), p. 253.

[27] I.L. Balandin , B.S. Bokstein , V.K Egorov, P.V. Kurkin: NanoStructured Materials. Vol. 8 (1997), p. 37.

[28] A. Portavoce, G. Chai, L. Chow, and J. Bernardini: J. Appl. Phys. Vol. 104 (2008), p. 104910.

[29] G. Hettich, H. Mehrer, and K. Maier: Inst. Phys. Conf. Ser. Vol. 46 (1979), p. 500.

[30] P. Dorner, W. Gust, B. Predel, U. Roll, A. Lodding, and H. Odelius: Philos. Mag. A Vol. 49 (1984), p. 557.

[31] Z. Balogh, Z. Erdélyi, D.L. Beke, A. Portavoce, C. Girardeaux, J. Bernardini, A. Rolland: Appl. Surf. Sci. Vol. 255 (2009), p. 4844.

[32] C. E. Allen, R. Ditchfield, and E. G. Seebauer: Phys. Rev. B Vol. 55 (1997) p. 13304.

[33] D. Mangelinck, K. Hoummada, A. Portavoce, C. Perrin, R. Daineche, M. Descoins, D. J. Larson, and P.H. Clifton: Scripta Materialia Vol. 62 (2010), p. 568.

[34] C. Perrin, K. Hoummada, I. Blum, A. Portavoce, M. Descoins, D. Mangelinck: Defect and Diffusion Forum Vols. 309-310 (2011), p. 161.

[35] M.K. Miller: *Atom Probe Tomography* (Kluwer Academic/Plenum Publisher, New York, 2000).

[36] R.G. Wilson, F.A. Stevie, and C.W. Magee, Secondary Ion Mass Spectrometry: a Practical Handbook for Depth Profiling and Bulk Impurity Analysis, Wiley, 1989.

[37] O. Moutanabbir, D. Isheim, D.N. Seidman, Y. Kawamura, and K.M. Itoh: Appl. Phys. Lett. Vol. 98 (2011), p. 013111.

[38] S. Ohsaki, K. Hono, H. Hidaka, and S. Takaki: Scripta Materialia Vol. 52 (2005), p. 271.

[39] K. Thompson, J.H. Booske, D.J. Larson, and T.F. Kelly: Appl. Phys. Lett. Vol. 87 (2005), p. 052108.

[40] E.A. Marquis, R. Hu, and T. Rousseau: J. Nucl. Mater. Vol. 413 (2011), p. 1.

[41] J. Weidow, and H.-O. Andrén: Acta Mater. Vol. 58 (2010), p. 3888.

[42] S. Duguay, A. Colin, D. Mathiot, P. Morin, and D. Blavette: J. Appl. Phys. Vol. 108 (2010), p. 034911.

[43] M.K. Miller, and M.G. Hetherington: Surf. Sci. Vol. 246 (1991), p. 442.

[44] F. Vurpillot, A. Bostel, and D. Blavette: Appl. Phys. Lett. Vol. 76 (2000), p. 3127.

[45] D. Blavette, P. Duval, L. Letellier, and M. Guttmann: Acta Mater. Vol. 44 (1996), p. 4995.

[46] F. De Geuser, W. Lefebvre, F. Danoix, F. Vurpillot, B. Forbord, and D. Blavette: Surface and Interface Analysis Vol. 39 (2007), p. 268.

[47] B. Gault, M. Müller, A. La Fontaine, M.P. Moody, A. Shariq, A. Cerezo, S.P. Ringer, and G.D. Smith: J. Appl. Phys. Vol. 108 (2010), p. 044904.

[48] P. Bas, A. Bostel, B. Deconihout, and D. Blavette: Appl. Surf. Sci. Vol. 87 (1995) p. 298.

[49] B. Bokstein, V. Ivanov, O. Oreshina, A. Peteline, S. Peteline: Mat. Sci. and Eng. Vol. A302 (2001), p. 151.

Recent Advances in Mass Transport in Materials
10.4028/www.scientific.net/DDF.322

Original Methods for Diffusion Measurements in Polycrystalline Thin Films
10.4028/www.scientific.net/DDF.322.129

DOI References
[4] N. Rodriguez, A. Portavoce, J. Delalleau, C. Grosjean, V. Serradeil, and C. Girardeaux: Thin Solid Films Vol. 518 (2010), p.5022.
doi:10.1016/j.tsf.2010.03.039

[5] P. Pichler, A. Burenkov, J. Lorenz, C. Kampen and L. Frey: Thin Solid Films Vol. 518 (2010), p.2478.
doi:10.1016/j.tsf.2009.09.150

[6] E.M. Bazizi, A. Pakfar, P.F. Fazzini, F. Cristiano, C. Tavernier, A. Claverie, N. Zographos, C. Zechner, and E. Scheid: Thin Solid Films Vol. 518 (2010), p.2427.
doi:10.1016/j.tsf.2009.09.141

[8] M. Pernach and M. Pietrzyk: Comput. Mater. Sci. Vol. 44 (2008), p.783.
doi:10.1016/j.commatsci.2008.05.035

[9] A. Portavoce, I. Blum, L. Chow, J. Bernardini, and D. Mangelinck: Defect and Diffusion Forum Vols. 309-310 (2011), p.63.
doi:10.4028/www.scientific.net/DDF.309-310.63

[10] A. Portavoce, R. Simola, D. Mangelinck, J. Bernardini1, and P. Fornara: Diffusion and Defect Data Vol. 264 (2007), p.33.
doi:10.4028/www.scientific.net/DDF.264.33

[11] A. Portavoce, D. Mangelinck, R. Simola, R. Daineche, and J. Bernardini: Defect and Diffusion Forum Vols. 289-292 (2009), p.329.
doi:10.4028/www.scientific.net/DDF.289-292.329

[12] A. Kikuchi and S. Sugaki: J. Appl. Phys. Vol. 53 (1982), p.3690.
doi:10.2465/ganko1941.77.65

[16] I. Blum, A. Portavoce, D. Mangelinck, R. Daineche, K. Hoummada, J.L. Lábár, V. Carron, and J. Bernardini: Microelectronic Engineering Vol. 87 (2010), p.263.
doi:10.1016/j.mee.2009.05.020

[20] H. Bakker, H. P. Bonzel, C. M. Bruff, M. A. Dayananda, W. Gust, J. Horváth, I. Kaur, G. V. Kidson, A. D. Le Claire, H. Mehrer, G. E. Murch, G. Neumann, N. Stolica, N. A. Stolwijk, in: Diffusion in Solid Metals and Alloys, Landolt-Börnstein-Numerical Data and Functional Relationships in Science and Technology, edited by H. Mehrer (Springer-Verlag, Berlin, 1990), Vol. 26.
doi:10.1007/10390457_26

[21] Y. Mishin, C. Herzig, J. Bernardini, and W. Gust: International Mat. Rev. Vol. 42 (1997), p.155.
doi:10.1179/095066097790093226

[24] L. G. Harrison: Trans. Faraday Soc. Vol. 57 (1961), p.1191.
doi:10.1039/tf9615701191

[25] A. Portavoce, L. Chow, and J. Bernardini: Appl. Phys. Lett. Vol. 96 (2010), p.214102.
doi:10.1063/1.3435476

[27] I.L. Balandin , B.S. Bokstein , V. K Egorov, P.V. Kurkin: NanoStructured Materials. Vol. 8 (1997), p.37.
doi:10.1016/S0965-9773(97)00063-9

[28] A. Portavoce, G. Chai, L. Chow, and J. Bernardini: J. Appl. Phys. Vol. 104 (2008), p.104910.
doi:10.1063/1.3010297

[30] P. Dorner, W. Gust, B. Predel, U. Roll, A. Lodding, and H. Odelius: Philos. Mag. A Vol. 49 (1984), p.557.
doi:10.1080/01418618408236556

[31] Z. Balogh, Z. Erdélyi, D.L. Beke, A. Portavoce, C. Girardeaux, J. Bernardini, A. Rolland: Appl. Surf. Sci. Vol. 255 (2009), p.4844.
doi:10.1016/j.apsusc.2008.12.010

[32] C. E. Allen, R. Ditchfield, and E. G. Seebauer: Phys. Rev. B Vol. 55 (1997) p.13304.
doi:10.1557/PROC-470-313

[33] D. Mangelinck, K. Hoummada, A. Portavoce, C. Perrin, R. Daineche, M. Descoins, D. J. Larson, and P.H. Clifton: Scripta Materialia Vol. 62 (2010), p.568.
doi:10.1016/j.scriptamat.2009.12.044

[34] C. Perrin, K. Hoummada, I. Blum, A. Portavoce, M. Descoins, D. Mangelinck: Defect and Diffusion Forum Vols. 309-310 (2011), p.161.
doi:10.4028/www.scientific.net/DDF.309-310.161

[37] O. Moutanabbir, D. Isheim, D.N. Seidman, Y. Kawamura, and K.M. Itoh: Appl. Phys. Lett. Vol. 98 (2011), p.013111.
doi:10.1063/1.3531816

[38] S. Ohsaki, K. Hono, H. Hidaka, and S. Takaki: Scripta Materialia Vol. 52 (2005), p.271.
doi:10.1016/j.scriptamat.2004.10.020

[40] E.A. Marquis, R. Hu, and T. Rousseau: J. Nucl. Mater. Vol. 413 (2011), p.1.
doi:10.1016/j.jnucmat.2011.03.023

[41] J. Weidow, and H. -O. Andrén: Acta Mater. Vol. 58 (2010), p.3888.
doi:10.1016/j.actamat.2010.03.038

[42] S. Duguay, A. Colin, D. Mathiot, P. Morin, and D. Blavette: J. Appl. Phys. Vol. 108 (2010), p.034911.
doi:10.1063/1.3466783

[43] M.K. Miller, and M.G. Hetherington: Surf. Sci. Vol. 246 (1991), p.442.
doi:10.1016/0039-6028(91)90449-3

[44] F. Vurpillot, A. Bostel, and D. Blavette: Appl. Phys. Lett. Vol. 76 (2000), p.3127.
doi:10.1016/S0304-3991(00)00035-8

[45] D. Blavette, P. Duval, L. Letellier, and M. Guttmann: Acta Mater. Vol. 44 (1996), p.4995.
doi:10.1016/S1359-6454(96)00087-0

[46] F. De Geuser, W. Lefebvre, F. Danoix, F. Vurpillot, B. Forbord, and D. Blavette: Surface and Interface Analysis Vol. 39 (2007), p.268.
doi:10.1002/sia.2489

[47] B. Gault, M. Müller, A. La Fontaine, M.P. Moody, A. Shariq, A. Cerezo, S.P. Ringer, and G.D. Smith: J. Appl. Phys. Vol. 108 (2010), p.044904.
doi:10.1063/1.3462399

[48] P. Bas, A. Bostel, B. Deconihout, and D. Blavette: Appl. Surf. Sci. Vol. 87 (1995) p.298.
doi:10.1016/0169-4332(94)00561-3

[49] B. Bokstein, V. Ivanov, O. Oreshina, A. Peteline, S. Peteline: Mat. Sci. and Eng. Vol. A302 (2001), p.151.
doi:10.1016/S0921-5093(00)01367-8